Synthesis, Biological Activity, and Structure−Activity Relationships for Potent Cytotoxic Rhodium(III) Polypyridyl Complexes

Melanie Harlos,[†] Ingo Ott,[‡] Ronald Gust,[‡] Hamed Alborzinia,[§] Stefan Wölfl,[§] Anna Kromm,[†] and William S. Sheldrick*,[†]

Lehrstuhl für Analytische Chemie, Ruhr-Universität Bochum, D-44780 Bochum, Germany, Institut für Pharmazie, Freie Universität Berlin, Königin-Luise-Strasse 2-4, D-14195 Berlin, Germany, and Institut für Pharmazie und Molekulare Biotechnologie, Ruprecht-Karls-Universität Heidelberg, Im Neuenheimerfeld 364, D-69120 Heidelberg, Germany

Received February 19, 2008

The complexes *mer*-[$RhCl_3$(DMSO-κS)(pp)] **1a**−**5a** may be prepared by reaction of *mer,cis*-[$RhCl_3$(DMSO-κS)$_2$(DMSO-κO)] with the appropriate polypyridyl ligand (pp = bpy, phen, dpq, dppz, dppn) in CH_3OH/H_2O solution at 75 °C. The *mer* isomers of **1a**−**5a** are stable in chloroform solution but those of **1a** and **2a** isomerize rapidly to a mixture of *fac* and *mer* isomers in DMSO. The complexes are potent in vitro cytotoxic agents and exhibit IC_{50} values that are strongly dependent on the size of the polypyridyl ligand. IC_{50} values of, respectively, 4.0 (0.5) and 1.9 (0.5), 0.40 (0.06) and 0.19 (0.05), and 0.079 (0.012) and 0.069 (0.021) μM are observed for **1a**−**3a** against the human cell lines MCF-7 (breast cancer) and HT-29 (colon cancer). Cellular uptake studies showed a rapid and high accumulation of the polypyridyl compounds. Treatment of HT-29 and MCF-7 cells with **3a** leads to significant decreases in cellular oxygen consumption and the rate of extracellular acidification.

Introduction

Although dirhodium(II, II) carboxylates have received considerable attention as anticancer agents[1–4] owing to their limited side effects, relatively few reports of cytotoxic rhodium(III) complexes have previously appeared. The trichloridorhodium(III) complexes *mer,cis*-[$RhCl_3$(DMSO-κS)$(Im)_2$] (DMSO = $(CH_3)_2SO$, Im = imidazole) and *mer,cis*-[$RhCl_3$(DMSO-κS)$_2$(L)] (L = Im, NH_3) were studied by Mestroni et al., who established a remarkable cytotoxic activity (IC_{50} = 1.5 ± 0.4, 0.4 ± 0.2, 9 μM) for the latter ammine complex toward the human cell lines A 2780 (ovarian carcinoma), LoVo (colon carcinoma), and Calu (lung carcinoma).[5] Replacing ammonia by imidazole leads to an increase in the IC_{50} values by about an order of magnitude and *mer,cis*-[$RhCl_3$(DMSO-κS)$(Im)_2$] is essentially inactive against A2780 and Calu (IC_{50} > 200 μM) and only moderately active toward the colon carcinoma cell line LoVo (IC_{50} = 40 ± 15 μM). Significant activity against mouse P 388 leukemia has, however, been reported for the analogous compound *mer,cis*-[$RhCl_3$(DMSO-κS)$(py)_2$] (py = pyridine).[6] The 2,2′:6′,2″-terpyridine (tpy) complexes *mer*-[$RhCl_3$(tpy)] and [Rh(Im)$(tpy)_2$]Cl·$3H_2O$ also exhibit potentially useful cytotoxicity,[7] as does the compound *fac*-[$RhCl_3$(9-[ane]-NS_2)] (9-[ane]-NS_2 = 1-aza-4,7-dithiacyclononane).[8a]

These findings suggest that octahedral trichloridorhodium(III) complexes could offer considerable scope for the development of anticancer agents. We have recently demonstrated that the cellular uptake and cytotoxicity toward the human cell lines MCF-7 (breast cancer) and HT-29 (colon cancer) for organoruthenium(II) complexes of the type [(η^6-C_6Me_6)RuCl(pp)]-(CF_3SO_3) are directly correlated to the size of the polypyridyl ligand.[9] A similar trend is observed for the cytotoxicities of analogous organometallic Rh(III) and Ir(III) complexes [(η^5-C_5Me_5)MCl(pp)](CF_3SO_3) (M = Rh, Ir),[10,11] and this finding prompted us to prepare and study the biological properties of trichloridorhodium(III) polypyridyl complexes. We chose the ligands bpy, phen, dpq, dppz, and dppn to generate a series of *mer*-complexes (Figure 1) with a steadily increasing aromatic surface area. Both *mer* and *fac* isomers are possible for the complexes of the type [$RhCl_3$(DMSO-κS)(pp)], and their cytotoxicities may well be expected to depend not only on the size of the polypyridyl ligand but also on the rate of ligand substitution in aqueous solution. The latter parameter will itself depend on both the general kinetic inertness of octahedral complexes of the group 9 metal (k(Rh) > k(Ir)) and on the specific *trans* effect of the constitutive ligands (DMSO-κS > Cl > pp-κN > H_2O). Nonorganometallic complexes of the heavier homologue iridium(III) are generally considered to be kinetically too inert to exhibit significant cytotoxicity and an absence of biological activity has indeed been confirmed for

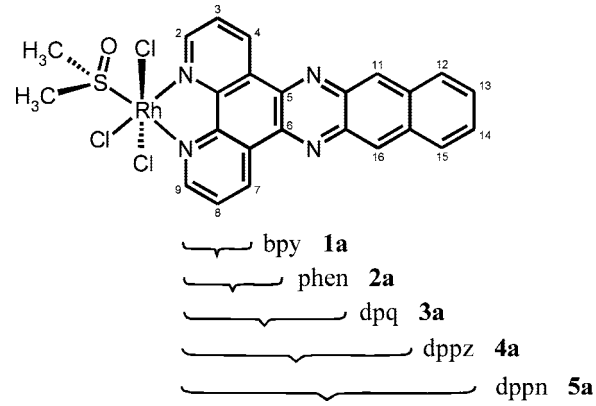

Figure 1. Structures of the trichloridorhodium(III) polypyridyl complexes *mer*-[$RhCl_3$(DMSO-κS)(pp)] **1a**−**5a** (pp = bpy, phen, dpq, dppz, dppn).

* To whom correspondence should be addressed. Phone: +49-234-3224192. Fax: +49-234-3214420. E-mail: william.sheldrick@rub.de.
† Ruhr-Universität Bochum.
‡ Freie Universität Berlin.
§ Ruprecht-Karls-Universität Heidelberg.

[a] Abbreviations: bpy, 2,2′-bipyridine; phen, 1,10-phenanthroline; dpq, dipyrido[3,2-*f*:2′,3′-*h*]quinoxaline; dppz, dipyrido[3,2-*a*:2′,3′-*c*]phenazine; dppn, benzo[i]dipyrido[3,2-*a*:2′,3′-*c*]phenazine; Im, imidazole; DMSO, dimethylsulfoxide; LSIMS, liquid secondary ion mass spectrometry; AAS, atomic absorption spectrometry; ISFETS, ion sensitive field effect transistors; IDES, interdigitated electrode structures

10.1021/jm800173s CCC: $40.75
Published on Web 06/11/2008

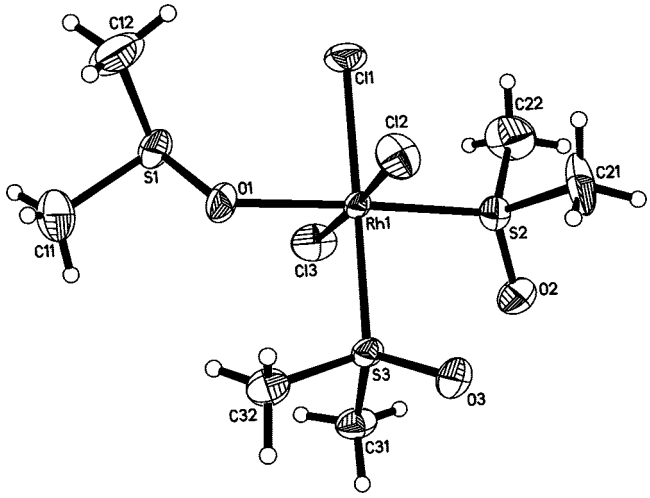

Figure 2. Molecular structure of *mer,cis*-[$RhCl_3$(DMSO-κS)$_2$(DMSO-κO)].

[ImH][*trans*-$IrCl_4$(DMSO-κS)(Im)] and [$(DMSO)_2H$][*trans*-$IrCl_4$-(DMSO-κS)$_2$].[12]

Results and Discussion

Synthesis. The rhodium(III) complexes *mer*-[$RhCl_3$(DMSO-κS)(pp)] **1a**−**5a** (pp = bpy, phen, dpq, dppz, dppn) were prepared by treatment of the precursor *mer,cis*-[$RhCl_3$(DMSO-κS)(DMSO-κO)][13–15] with an equivalent of the appropriate polypyridyl ligand in CH_3OH/H_2O solution (1/1). The presence of a single isomer is confirmed in each case by the observation of just one strong νSO band (values 1130−1118 cm^{-1}) in the typical range 1100−1150 cm^{-1}. Although the precursor was prepared in accordance with the literature procedure by reaction of $RhCl_3 \cdot 3H_2O$ with DMSO followed by addition of ethanol to achieve precipitation,[14] we obtained a novel monoclinic polymorph on crystallization of *mer,cis*-[$RhCl_3$(DMSO-κS)$_2$-(DMSOκO)] by slow evaporation of a CH_3OH/H_2O solution. Both polymorphs crystallize in the space group $P2_1/c$ but exhibit very different unit cell constants and packing arrangements. The structure of the new polymorph is depicted in Figure 2. As a result of the stronger *trans* influence of the chloride ligand Cl1 in comparison to the O1 atom of the κO DMSO ligand, the Rh1−S3 bond length of 2.305(2) Å is significantly longer than that of Rh1−S2 [2.256(2) Å]. An Rh1−O1 distance of 2.113(5) Å is observed for the κO DMSO ligand.

The ^{1}H NMR spectrum for the *mer* complex **5a** (pp = dppn) in $CDCl_3$ solution is depicted in Figure 3 as a typical example for the rhodium(III) polypyridyl complexes. As a result of the stronger *trans* influence of the κS DMSO ligand, the resonances for the protons H7−H9 are shifted significantly (0.06−0.09 ppm) to lower field in comparison to H2−H4 of the pyridine ring sited *trans* to a chloride ligand. Confirmation of the κS coordination of the DMSO ligands in **1a**−**5a** is provided by the pronounced downfield shift of their methyl ^{1}H NMR resonances to 3.71−3.84 ppm in comparison to the signal of free DMSO at 2.55 ppm. Whereas *mer,cis*-[$RhCl_3$(DMSO-κS)$_2$(DMSO-κO)] exhibits similar marked shifts to 3.62 (*trans* to DMSO-κO) and 3.44 (*trans* to Cl) for its κS DMSO ligands, only a modest lowfield shift to 2.86 ppm is observed for its κO DMSO ligand in $CDCl_3$.[14]

The *mer* complexes **1a**−**5a** are all stable in $CDCl_3$ solution over a period of 24 h at 25 °C in the presence of light, in contrast to their solutions in DMSO. Rapid isomerization to mixtures of the *mer* and *fac* isomers (Figure 4) **1a/1b** (29:71) and **2a/2b** (60:40) is observed for solutions of **1a** and **2a** after 15 min in DMSO. Equilibration is much slower for **3a**–**5a**, e.g. **3a/3b** are present in a 75:25 ratio in DMSO after 24 h. As depicted for the **1a/1b** mixture in Figure 5, the protons H2/H9, H3/H8, H4/H7 and H5/H6 are magnetically equivalent for the C_s symmetrical *fac* isomers. A marked upfield shift from two separate doublets at 9.78 and 9.83 ppm to a common doublet at 9.47 ppm is observed for the H2 and H9 protons of **1a** on isomerization to **1b**. The average positions for the remaining bpy protons remain effectively unchanged on going from **1a** to **1b**. We were successful in crystallizing the latter *fac* isomer **1b** (Figure 6) on slow evaporation of a CH_3OH/H_2O solution of the original *mer* isomer **1a**. The relative strength of the *trans* influence of the κS DMSO ligand can be gauged in **1b** by comparing the length of Rh1−Cl1 with Rh1−Cl2 and Rh1−Cl3. The former bond [2.366(1) Å] is significantly longer than the latter bonds [2.332(1), 2.349(1) Å] in *trans* position to the bpy nitrogen atoms N1 and N10.

Rapid isomerization to equilibrium mixtures of *mer* and *fac* isomers is also observed on dissolving **1a** and **2a** in the polar solvents CD_3OD and D_2O. This is accompanied by a limited degree of slow DMSO/CH_3OD exchange in methanol and almost complete rapid DMSO substitution in aqueous solution. The observed ^{1}H NMR ratios of coordinated DMSO to free DMSO are 95:5 and 93:7 for the bpy and phen complexes in methanol after 24 h and 5:95 and 14:86 in water after 5 min. This indicates that aquation to *mer/fac*-[$RhCl_3(H_2O)$(pp)] will be rapid in biological systems and that the aqua complexes will be the potentially biologically relevant species. Registration of satisfactory ^{1}H NMR spectra of **3a**−**5a** in CD_3OD or D_2O was prevented by their poor solubility. The compound [$RhCl_3$(DMSO-κS)(1,4-dithiane-$\kappa^2 S,S$)] **6** containing the cyclic bidentate 1,4-dithiane ligand $(CH_2CH_2S)_2$ was prepared for comparison purposes. Its ^{1}H NMR spectrum in $CDCl_3$ contains two resonances of approximately equal integral intensity for DMSO methyl protons at 3.43 and 3.55 and is, therefore, in accordance with the presence of a 1:1 mixture of the *mer* and *fac* isomers in solution.

Interaction with DNA. We have demonstrated that organometallic complexes of the types [(η^5-C_5Me_5)Ir(L)(dppz)](CF_3SO_3)$_2$[11,16,17] and [(η^6-C_6Me_6)Ru(L)(dppz)]$(CF_3SO_3)_2$[9,18] (L = $(NH_2)_2CS$, methionyl peptides) are strong metallointercalators for DNA with binding constants in the range 10^5−10^7 M^{-1}. A significant degree of intercalation is also observed for complexes containing the smaller dpq ligand but not for those of phen[16,11] or dppn,[9,11] which are apparently respectively too short or too long to facilitate effective side-on intercalation between the nucleobases of the double helix.[16,18] Rapid substitution of the chloride ligand by nucleobase N atoms leads to stable covalent DNA binding for [(η^5-C_5Me_5)IrCl(dppz)](CF_3SO_3) following initial kinetically favored intercalation.[11] It was, therefore, of interest to study the DNA interaction of the *mer* complexes **1a**−**5a**, in which the facial [η^5-C_5Me_5]$^-$ coligand is replaced by three kinetically relatively inert chloride ligands and a labile DMSO, and the 5d transition metal is replaced by its lighter 4d homologue. A pronounced decrease in UV/vis absorbance and bathochromic shifts for the absorption maxima at about 364 and 383 nm on addition of dppz-containing metal complexes to calf thymus DNA are generally indicative of possible dppz intercalation. However, only negligible changes are observed for the absorbances of these maxima, when the UV/vis spectrum of a 20 μM aqueous solution of **4a** is recorded with and without CT DNA (M(nucleotide) = 200 μM). The UV/vis spectra for

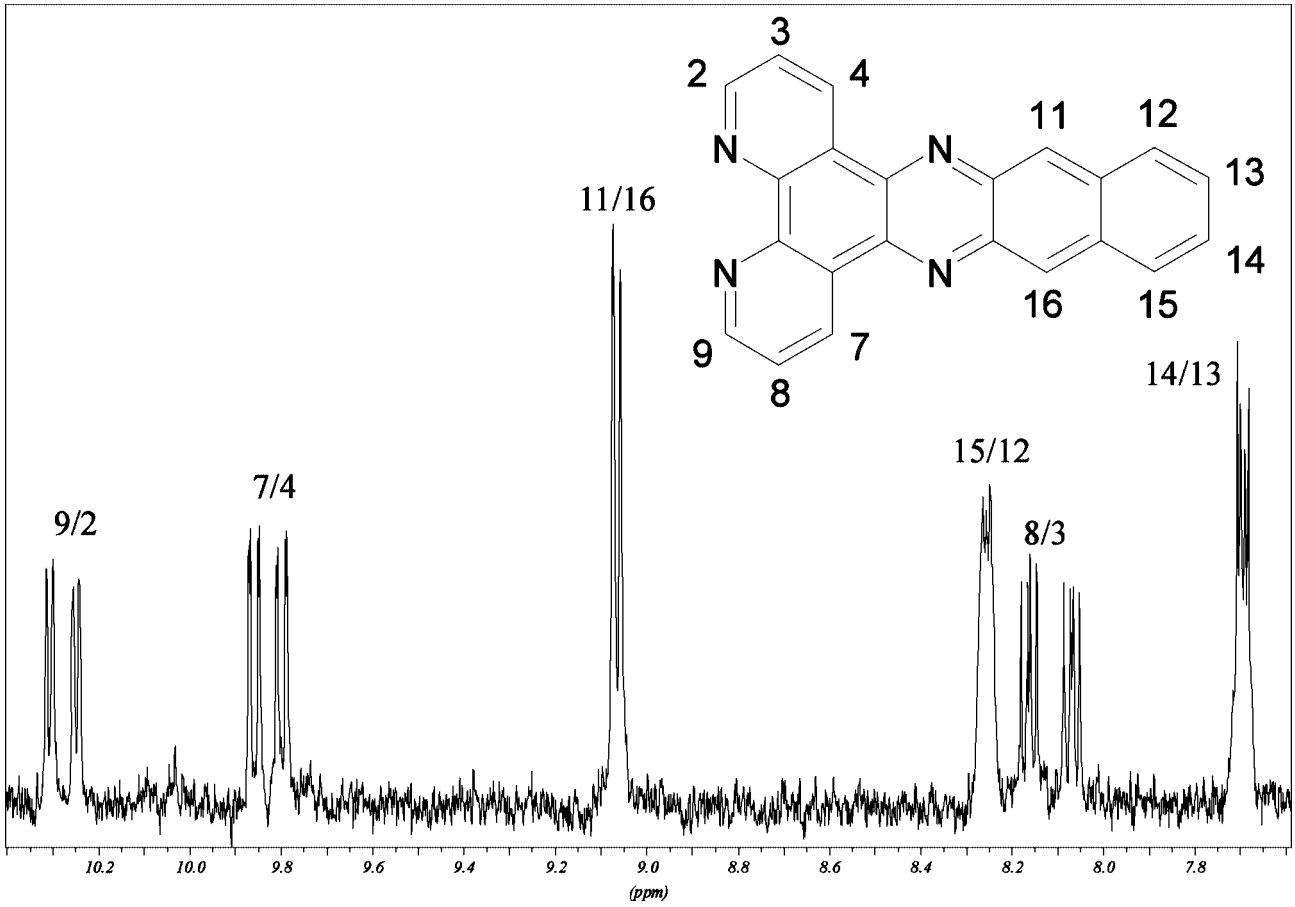

Figure 3. Aromatic region of the ^{1}H NMR spectrum of *mer*-[$RhCl_3$(DMSO-κS)(dppn)] (**5a**) in $CDCl_3$ solution.

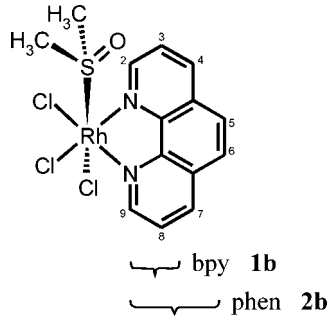

Figure 4. Structures of the *fac* isomers *fac*-[$RhCl_3$(DMSO-κS)(pp)] **1b** (pp = bpy) and **2b** (pp = phen).

the other complexes **1a**−**3a** and **5a** also exhibit no effective changes in absorption on mixing with CT DNA.

Characteristic changes in the circular dichroism (CD) spectra of DNA in the presence of small molecules can provide a means of monitoring possible conformational changes for the biopolymer.[19,20] Aromatic molecules often generate CD bands between 300 and 400 nm on interaction with DNA, as a result of intercalation, surface or groove binding leading to a rigid orientation of their dipole moments with respect to the double helix. We have reported, in this context, that organoiridium(III) and organoruthenium(II) dppz complexes exhibit characteristic induced negative CD bands at $\lambda = 300$ nm on intercalation into DNA[9,11,17] and that a decrease in the molar elipticity [θ] of the positive DNA band in the range 270 − 290 nm can be indicative of dpq intercalation.[9] Figure S2 of the Supporting Information depicts the CD spectrum for a mixture of **4a** with CT DNA at $r = 0.1$ (r = [**4a**]/[DNA]) in a 10 mM phosphate buffer after an incubation period of 2 h. The molar elipticities [θ] of the typical negative and positive DNA bands are similar to those observed for DNA alone and the lack of a negative CD band at 300 nm is in accordance with an absence of dppz intercalation as indicated by the UV/vis studies. The characteristic DNA CD spectrum also remains effectively unchanged on treatment with the other *mer* complexes **1a**−**3a** and **5a**.

In view of the apparent absence of DNA intercalation for **3a** and **4a**, we also studied the possibility of a coordination of the rhodium complexes by nucleobase N atoms. To this purpose, the possible reaction of a 10 mM solution of complex **1a** with a 2-fold excess of guanosine 5′-monophosphate in a 10 mM phosphate buffer (pH = 7.2) was monitored by ^{1}H NMR spectroscopy. In contrast to (η^5-C_5Me_5)Ir(III) polypyridyl complexes [(η^5-C_5Me_5)IrCl(pp)]$^+$, for which the formation of $\kappa N7$ (guanine) complexes is very rapid at 25 °C,[14] no reaction with the nucleobase was observed for **1a** even after treatment at 60 °C for 72 h. Our findings therefore suggest that neither intercalation nor covalent binding to DNA may be of significance for the cellular activity of the complexes. The overall neutrality of the complexes may be assumed to be responsible for the absence of effective intercalation by **3a** and **4a**, whose aromatic dpq and dppz ligands would clearly offer suitable surface areas for this DNA binding mode.

Cytotoxicity and Cellular Uptake. Table 1 lists the in vitro cytotoxicity of complexes **1a**−**5a** and **6** toward the human cancer cell lines MCF-7 (breast cancer) and HT-29 (colon cancer). It is apparent for the complexes **1a**−**3a** that their IC_{50} values (bpy > phen > dpq) are strongly correlated to the surface area of the polypyridyl ligand. We have reported a similar trend for the organometallic complexes [(η^5-C_5Me_5)RuCl(pp)](CF_3-

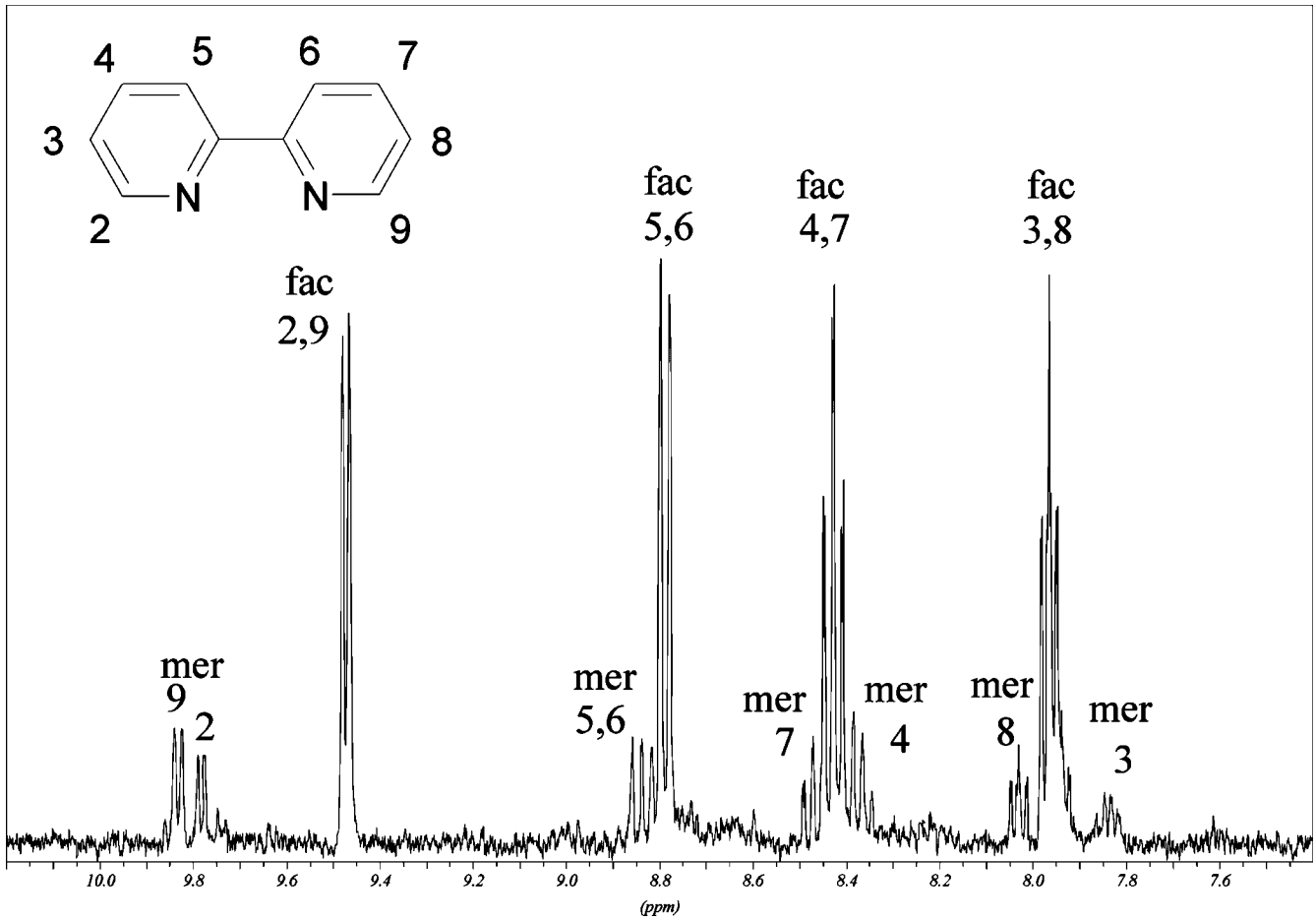

Figure 5. ^{1}H NMR spectrum of the mixture of isomers *mer*-[$RhCl_3$(DMSO-κS)(bpy)] **1a** and *fac*-[$RhCl_3$(DMSO-κS)(bpy)]**1b** in DMSO-d_6 solution.

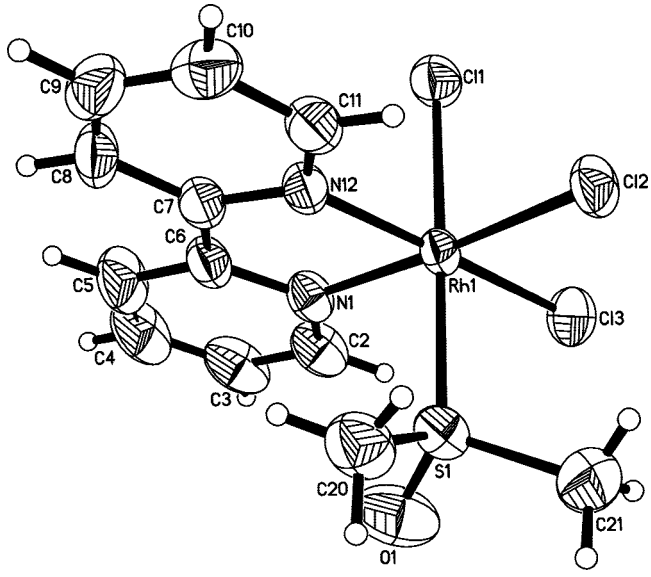

Figure 6. Molecular structure of *fac*-[$RhCl_3$(DMSO-κS)(bpy)] **1b**.

SO_3),[9] where the IC_{50} values for MCF-7 and HT-29 cells improve from 11.1 (1.0) and 30.3 (5.6) for pp = dpq over 2.1 (0.6) and 2.5 (0.6) for pp = dppz to 0.13 (0.02) and 0.4 (0.1) μM for pp = dppn. In contrast, whereas a dramatic improvement is observed for the smaller bpy, phen and dpq ligands of **1a**−**3a**, no further significant increase in cytotoxicity is apparent for the larger dppz and dppn ligands of **4a** and **5a** (Figure S3 of the Supporting Information). A size dependence is also apparent for the relative activity of the complexes toward the different cell lines. Whereas **1a** and **2a** are about twice as active toward HT-29 cells, much smaller relative differences are observed for **3a** and **4a**, and complex **5a** with the largest polypyridyl ligand is slightly more active toward MCF-7 cells. Replacement of the polypyridyl ligand with dithiane (**6**) caused significantly higher IC_{50}-values. Complexes **3a**−**5a** are extremely potent cytotoxic agents with IC_{50} values in the range 0.069−0.079 μM, that are some 2 orders of magnitude lower than for cisplatin. In this context, it should be noted that we also observed toxic effects for the free polypyridyl ligands, which increase in the series bpy < phen, dpq < dppz < dppn. However, the corresponding complexes **1a**−**5a** displayed significantly higher activity in all the experiments. For the larger free polypyridyl ligands (dppz and dppn), limited solubility in the assay media was noted, which might limit their bioavailability.

Table 1. IC_{50} Values (μM) for the Complexes *mer*-[$RhCl_3$(DMSO)(pp)] **1a**−**6** and Corresponding Free Polypyridyl Ligands in MCF-7 and HT-29 Cells; n.d.: Not Determined

		MCF-7 IC_{50}		HT-29 IC_{50}	
complex	pp	complex	ligand	complex	ligand
1a	bpy	4.0(0.5)	52.7(7.8)	1.9(0.5)	45.7(4.6)
2a	phen	0.40(0.06)	3.5(0.2)	0.19(0.05)	2.7(0.5)
3a	dpq	0.079(0.012)	6.7(2.0)	0.069(0.021)	7.0(2.2)
4a	dppz	0.095(0.020)	0.8(0.6)	0.073(0.017)	1.8(0.2)
5a	dppn	0.051(0.012)	0.15(0.05)	0.070(0.008)	n.d.
6	$S_2(CH_2)_4$	9.0(0.5)	n.d.	16.5(6.5)	n.d.
cisplatin		2.0(0.3)		7.0(2.0)	

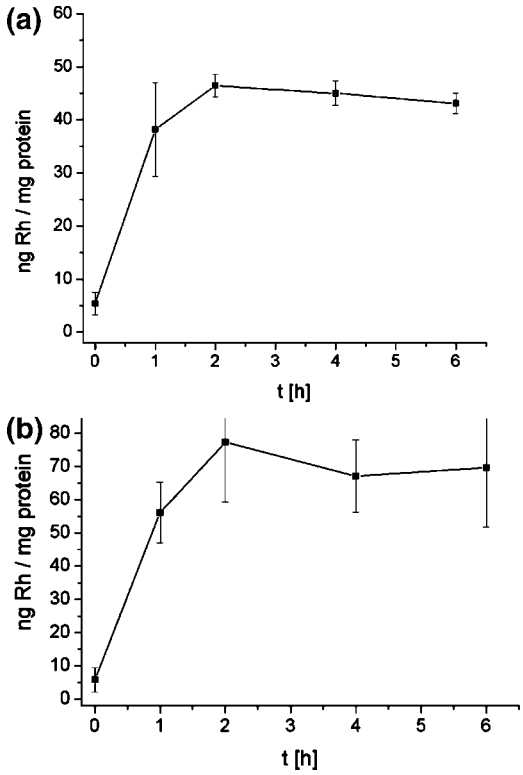

Figure 7. Time dependent uptake of 1.0 μM **4a** into (a) MCF-7 cells and (b) HT-29 cells.

Extending the size of the polypyridyl ligand will confer lipophilic character to the complexes and thereby enhance their passage through the cell membrane. The neutrality of complexes **1a**−**5a** and **6** should also favor cellular uptake. A quantitative AAS study[9] for the complexes $[(\eta^6\text{-}C_6Me_6)RuCl(pp)](CF_3SO_3)$ has demonstrated that the Ru uptake increases dramatically in the order dpq < dppz < dppn from 1.1 (1.1) and 11.8 (8.5) ng Ru/mg protein for the dpq complex to 906.7 (1.5) and 1054.7 (94.5) ng Ru/mg protein for the dppn complex. An analysis of the IC_{50} values listed in Table 1 suggests that an increase in intracellular concentration on going from **1a** to **3a** could lead to the observed dramatic increase in cytotoxicity for the series and that a saturation level may be achieved for pp = dpq. Further increases in the lipophilicity for **4a** and **5a** have apparently no additional beneficial influence on the cytotoxic cellular activity of the complexes. To evaluate the uptake charactaristics of the target compounds **1a**−**5a**, we determined the Rh levels of tumor cells exposed to the compounds by atomic absorption spectroscopy. Initial experiments were performed exemplarily on the dppz compound **4a**. On incubation with 1.0 μM of **4a**, cellular Rh levels increased quickly within the first two hours of exposure (Figure 7). Longer incubation periods afforded no significant changes, which indicates that following a rapid uptake process essentially stable cellular levels were reached. A slight though not significant trend to lower uptake values is apparent for the measurements after 4 and 6 h. Exposure to various concentrations of **4a** (0.2−5.0 μM) for 6 h led to an almost linear increase ($r^2 > 0.99$) of the cellular rhodium(III) level (Figure 8). This demonstrates that the plateau levels in Figure 7 are not the consequence of a saturation effect for the cellular uptake process.

On the basis of these results, the tumor cells were exposed to 1.0 μM of **1a**−**5a** and **6** for 6 h for the celluar uptake measurements reported in Table 2. On taking the cytotoxic activities of the compounds into account, an increase of cellular

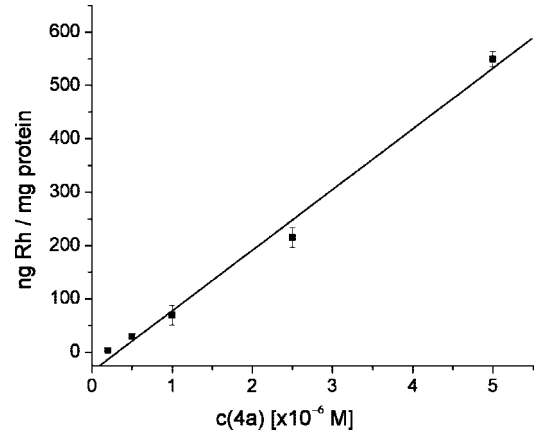

Figure 8. Concentration dependence of the uptake of **4a** into MCF-7 cells.

Table 2. Cellular Uptake (ng Rh/mg Cell Protein) in MCF-7 and HT-29 Cells for 1.0 μM of the Complexes *mer*-$[RhCl_3(DMSO)(pp)]$ **1a**−**6**

Complex	pp	MCF-7	HT-29
1a	bpy	41.6(0.5)	24.7(9.2)
2a	phen	70.8(12.2)	49.0(0.6)
3a	dpq	92.1(1.4)	53.6(2.0)
4a	dppz	43.1(1.9)	69.8(18)
5a	dppn	74.7(1.7)	39.8(9.7)
6	$S_2(CH_2)_4$	10.5(1.7)	13.3(2.1)

Rh levels in the order **6** < **1a** < **2a** < **3a** ≈ **4a** ≈ **5a** was to be expected. This trend was only observed in part. On the one hand, a lower level of cellular uptake was indeed observed for the less toxic compounds **1a** and **6**, but on the other hand, the accumulation of **2a** was comparable to that of the more toxic complexes **3a**−**5a**. With the exception of **6** and **4a**, higher ng Rh/mg protein levels were reached in MCF-7 cells in comparison to HT-29 cells. However, on taking the individual cellular parameters into account (e.g., the mean cellular diameter and the mean protein to volume ratio of HT-29[21] and MCF-7[22] cells), it can be estimated that 1.0 ng Rh per mg protein corrrespond to a cellular molar concentration of 1.9 μM in HT-29 cells but to only 1.1 μM in MCF-7 cells. Thus, **1a**−**3a** and **5a** reached comparable molar levels in both studied cell lines. For example, the cellular molar concentration of **5a** was 82 μM in MCF-7 cells and 76 μM in HT-29 cells.

The observed cellular uptake values can be classified as very high when compared to those of other established metallodrugs. In the present study, the highest molar cellular concentration (133 μM) was observed for **4a** in HT-29 cells. With respect to the exposure concentration of 1.0 μM, this means that the compound is accumulated 133 fold in the cancer cells! In comparison, similar studies on the cellular uptake of the clinically used platinum drugs cisplatin, carboplatin, and oxaliplatin have shown that these complexes are accumulated only 1.5−6 fold.[23]

Cellular Metabolism and Morphological Changes. We have studied the cellular metabolism and morphological changes of HT-29 and MCF-7 cells in response to the highly cytotoxic compounds **3a** and **4a** with a cell-based sensor chip system, which has the ability to monitor the biological impact of a compound by measuring three important parameters of cellular metabolism in living cell cultures. These parameters are oxygen consumption, the extracellular acidification rate, and changes in cellular adhesion or morphology. The metabolic silicon chip includes miniature Clark-type oxygen electrodes for monitoring the cellular oxygen uptake,[24] ion-sensitive field effect transistors

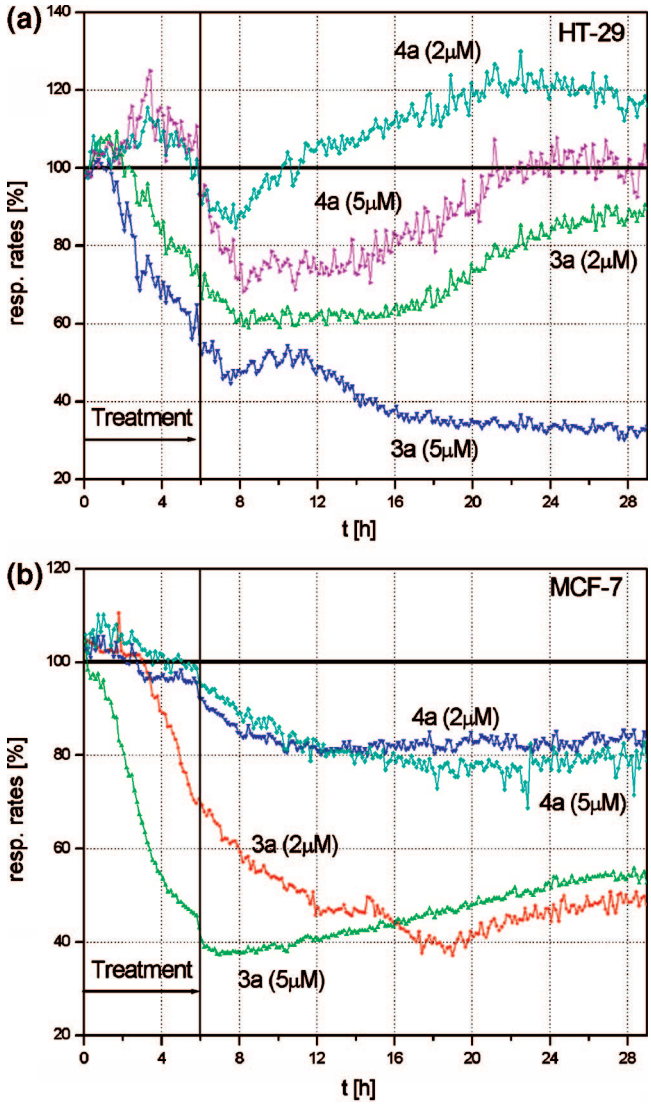

Figure 9. Standard respiration rates (%) for (a) HT-29 cells and (b) MCF-7 cells treated with 2 and 5 μM solutions of compounds **3a** and **4a** over the period 0−6 h. The end of treatment is indicated by a vertical line. Measurement was continued for an additional 24 h (6−30 h) after removal of substances.

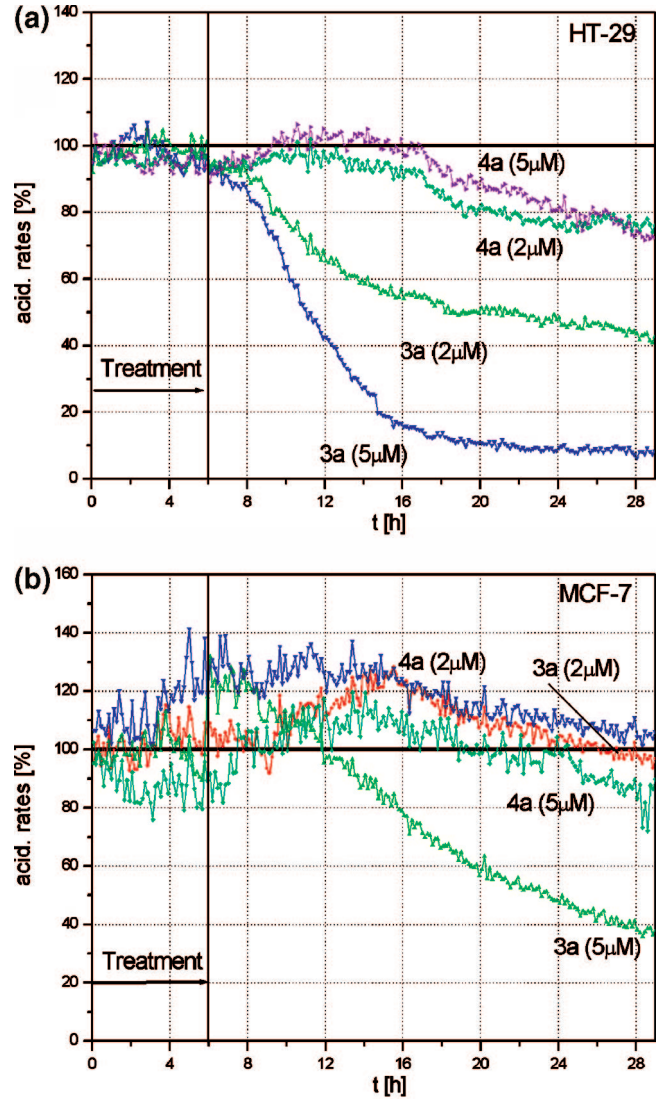

Figure 10. Standard extracellular acidification rates (%) for (a) HT-29 cells and (b) MCF-7 cells treated with 2 and 5 μM solutions of compounds **3a** and **4a** over the period 0−6 h. The end of treatment is indicated by a vertical line. Measurement was continued for an additional 24 h (6−30 h) after removal of substances.

to record extracellular pH changes,[22] and interdigitated electrode structures for measuring the cellular impedance.[26] Oxygen consumption and acidification rate are important parameters for identifying the contribution of glycolysis and mitochondrial respiration to the energy metabolism of the cells.

Oxygen consumption is generally indicative of enhanced or decreased mitochondrial activity (respiration). Other oxygen consuming processes are much less efficient and thus unlikely to contribute significantly to this signal. From Figure 9a, it is apparent that the oxygen consumption of HT-29 cells is strongly affected during the first hours of treatment with **3a**. For a 2 μM solution of the complex, a rapid initial decrease to a 60% level is observed, followed by a degree of recovery during the regeneration phase after 12 h. In contrast, regeneration is no longer visible for the 5 μM solution of **3a**, possibly due to permanent damage of the mitochondria. Both the 2 and 5 μM concentrations have similar effects on the respiration rates for HT-29 cells treated with complex **4a**. After small positive and negative fluctuations in oxygen consumption, the signal values approach the control levels during the regeneration phase. The respiration rate of MCF-7 cells (Figure 9b) is rapidly affected by **3a** during the treatment phase and sinks to about 40% for both doses (2 and 5 μM) during the regeneration phase. Only a very limited increase is observed at both concentrations of **3a**. MCF-7 cells are more affected by **4a** than HT-29 cells with oxygen consumption falling to about 80% for both 2 and 5 μM concentrations of the compound.

Extracellular acidification is closely linked to the activity of glycolysis. This parameter is chiefly influenced by lactic acid production, which is the waste product of anaerobic metabolism. Within the first 10 h (6−16 h) following the treatment phase, a significant dose dependent decrease in the extracellular acidification rate is apparent for HT-29 cells treated with complex **3a** (Figure 10a), and interestingly this starts before treatment is stopped, which indicates permanent cellular damage associated with the high cytotoxicity of the compound. The marked reduction in lactic acid production is indicative of a much lower cellular activity in comparison to the nontreated cells. Treatment of MCF-7 cells with **3a** at a 5 μM concentration reduces the acidification rate to 40% after 28 h, but the compound has little effect at a lower 2

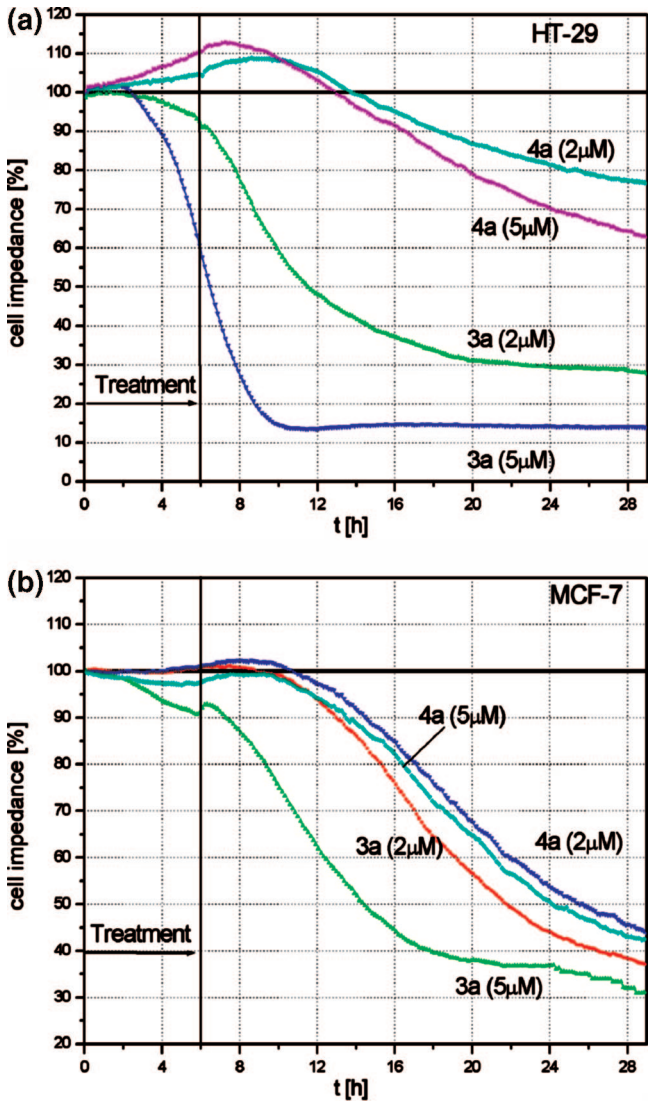

Figure 11. Standard cell impedance (%) for (a) HT-29 cells and (b) MCF-7 cells treated with 2 μM and 5 μM solutions of compounds **3a** and **4a** over the period 0−6 h. The end of treatment is indicated by a vertical line. Measurement was continued for an additional 24 h (6−30 h) after removal of substances.

μM concentration (Figure 10b). The impact of complex **4a** is much weaker for both cell lines, in particular for MCF-7, where the acidification rate is close to 100% after 28 h. This indicates that MCF-7 cells depend more on glycolysis for energy production in response to treatment with the rhodium(III) compounds.

IDES measurements of cellular impedance reflect the insulating properties of the cell membrane. Morphological changes and the status of cellular adhesion properties, including cell−cell and cell−matrix contacts are also monitored by cell impedance. The impedance signal for HT-29 and MCF-7 cells with a 5 μM solution of **3a** decreases rapidly after a period of approximately 3−4 h (Figure 11a,b) from commencement of treatment, whereas the impact of the 2 μM solution is somewhat less pronounced and delayed by a further 2−4 h in comparison. Complex **4a** also causes a significant though somewhat smaller decrease in cellular impedance for HT-29 and MCF-7 cells, but the onset of the effect is delayed for about 6 h after the end of treatment. The decline in cell impedance now takes place during the regeneration phase, which indicates the presence of permanent dose dependent cellular damage.

Conclusions

The complexes *mer*-[$RhCl_3$(DMSO-κS)(pp)] are potent cytotoxic agents toward the human cell lines MCF-7 and HT-29 and exhibit IC_{50} values in the range 0.069−0.079 μM for the larger polypyridyl ligands dpq, dppz, and dppn. A strong dependence on the surface area of the polypyridyl ligands and thereby on the compound lipophilicity and/or the *mer*/*fac* ratio in solution is apparent for the cytotoxicities of **1a**−**3a**, whose IC_{50} values decrease from 4.0 (0.5) and 1.9 (0.5) μM to 0.079 (0.012) and 0.069 (0.021) μM on going from pp = bpy (**1a**) to pp = dpq (**3a**). The latter value for HT-29 is some 2 orders of magnitude lower than that of 7.0 (2.0) μM determined for cisplatin.

Cellular uptake studies revealed high cellular levels of the target compounds, which correlated in part to the extent of the antiproliferative effects triggered by the complexes. The expected increase of cellular uptake levels on going to the larger polypyridyl ligands dppz and dppn could not be observed, which might provide an explanation for the fact that the toxicities of **3a**−**5a** did not differ significantly from one another. However, the impact of the pp ligands on the biological activity is demonstrated by results obtained with **6**, which was used as a reference substance not containing a pp ligand. In this case, much lower cellular uptake values were obtained and these correlate with elevated IC_{50} values of 9.0(0.5) and 16.5(6.5) μM for the compound in the cell growth assay.

Our ^{1}H NMR studies indicate that DMSO substitution is rapid for **1a**−**5a** in aqueous solution and that complexes of the type *mer*-[$RhCl_3(H_2O)$(pp)] will probably be the biologically active species. On the basis of our UV/vis and CD investigations, DNA may not be an important cellular target for these aqua complexes. In view of the rapid aquation of the original complexes **1a**−**5a**, it is possible that the hard carboxylate O atoms of aspartate or glutamate side chains or the hydroxy functions of serine or threonine residues could offer the central Rh(III) atom attractive coordination sites in intracellular proteins.

Studies on the cellular metabolism and morphological properties were exemplarily performed on **3a** and **4a** and showed that all measured parameters (cellular oxygen uptake, extracellular pH changes, and cellular impedance) were influenced by the presence of the complexes. However, the effects were in general more marked for **3a**. In particular, the strong effects of **3a** on cellular oxygen consumption are of special interest as they might indicate an antimitochondrial mode of action. This is in line with the results of a recently published study showing that Rh intercalators can lead to (oxidative) damage of mitochondrial DNA.[27]

The impedance measurements indicate that a modification of the cellular adhesion properties most probably contributes to the biological activity of the compounds. On the basis of the high cellular uptake rates noted for the complexes it appears reasonable that a significant quantity of the agents is accumulated in the lipophilic membrane environment and causes morphological changes.

Experimental Section

Materials and Instrumentation. UV/vis spectra were recorded with an Analytik Jena SPECORD 200 spectrometer and FTIR spectra with a Perkin-Elmer 1760X as KBr discs. A Jasco J-715 instrument was employed to measure CD spectra in the range 220−500 nm for 1:10 complex/[DNA] mixtures [complex = 20 μM, DNA concentration in M(nucleotide) = 200 μM] in a 10 mM

phosphate buffer at pH 7.2. Then 1% DMSO was added to ensure solubility of **1a**−**5a**. LSIMS spectra were registered for the mass range $m/z < 3000$ with a Fisons VG autospec employing a cesium ion gun (voltage 17 kV) and 3-nitrobenzyl alcohol as the liquid matrix. A Bruker DRX 400 was employed for the registration of ^{1}H and ^{13}C NMR spectra with chemical shifts reported as δ values relative to the signal of tetramethylsilane. Atomic absorption spectrometric measurements were performed on a Vario 6 (Analytik Jena) and elemental analyses on a Vario EL (Elementar Analysensysteme). $RhCl_3 \cdot 3H_2O$ was purchased from Chempur, phen from Acros, and bpy and DMSO from J. T. Baker. The polypyridyl ligands dpq,[28] dppz,[29] and dppn[30] were prepared in accordance with literature procedures as was the starting compound *mer,cis*-[$RhCl_3$-(DMSO-κS)$_2$(DMSO-κO)].[14]

X-ray Structural Analyses. Intensity data for *mer,cis*-[$RhCl_3$-(DMSO-κS)$_2$(DMSO-κO)] and *fac*-[$RhCl_3$(DMSO-κS)(bpy)]$\cdot H_2O$ **1b** were collected using ω scans on a Siemens P4 diffractometer equipped with graphite-monochromated Mo Kα radiation (λ = 0.71073 Å, $4° \leq 2\theta \leq 50°$). The data were corrected semiempirically for absorption (Ψ scans), and the structures were solved by direct methods and refined by full-matrix least-squares against F_0^2 using SHELX97.[31] Anisotropic temperature factors were employed for the non-hydrogen atoms with the exception of the disordered water oxygen atom of **1** and protons were included at geometrically calculated positions as riding atoms. The final R factors were respectively $R_1 = 0.047$ and 0.033 for $I > 2\sigma(I)$ with w$R_2 = 0.119$ and 0.083 for all independent reflections. CCDC 677679 and 677680 contain the supplementary crystallographic data for *mer,cis*-[$RhCl_3$(DMSO-κS)$_2$(DMSO-κO)] and **1b** and may be obtained free of charge at www.ccdc.cam.ac.uk/conts/retrieving.html or from the Cambridge Crystallographic Data Centre, 12 Union Road, Cambridge CB2 1EZ, U.K. (fax: int. code +44(0)1223/336−033, E-mail: deposit@chemcrys.cam.ac.uk).

Synthesis. Complexes **1a**−**5a** were prepared by displacing *cis*-sited DMSO and chloride ligands in *mer,cis*-[$RhCl_3$(DMSO-κS)$_2$(DMSO-κO)] with the appropriate polypyridyl ligand in CH_3OH/H_2O solution at 75 °C. The general procedure is described below for **1a**.

***mer*-[RhCl$_3$(DMSO)(bpy)] 1a.** *mer,cis*-[$RhCl_3$(DMSO-κO)(DMSO-κS)$_2$] (200 mg, 0.45 mmol) was dissolved in 10 mL of a 1:1 mixture of methanol and water. After addition of 2,2′-bipyridine (70.3 mg, 0.45 mmol), the reaction mixture was stirred for 2 h at 75 °C and then left to stand at 4 °C for a further 24 h. The resulting yellow precipitate was filtered off, treated with 5 mL of methanol, and reprecipitated by addition of diethyl ether. The solid was filtered off, washed and dried in vacuo. Yield: 76%. Anal. ($C_{12}H_{14}Cl_3N_2ORhS$) C, H, N. LSIMS: m/z (%) 407(100) [M − Cl]$^+$, 372(37) [M − 2Cl]$^+$. ^{1}H NMR ($CDCl_3$) δ: 3.71 (s, 6H, CH_3), 7.63 (dd, 1H), 7.71 (dd, 1H), 8.04 (dd, 1H), 8.11 (d, 1H) 8.14 (dd, 1H), 8.16 (d, 1H), 10.01 (d, 2H). IR: $\tilde{\nu}$ = 1126 s (νSO) cm^{-1}. Crystals of *fac*-[$RhCl_3$(DMSO-κS)(bpy)]$\cdot H_2O$ **1b** suitable for X-ray analysis were grown over a period of 7 days by slow evaporation of a solution of **1a** in water/methanol.

***mer*-[RhCl$_3$(DMSO)(phen)]$\cdot$H$_2$O 2a.** Synthesis as for **1a** with 1,10-phenanthroline (81.1 mg, 0.45 mmol). Yield: 74%. Anal. ($C_{14}H_{16}Cl_3N_2O_2RhS$) C, H, N. LSIMS: m/z (%) 431(100) [M − Cl]$^+$, 391(38) [M − 2Cl]$^+$. ^{1}H NMR ($CDCl_3$) δ: 3.78 (s, 6H, CH_3), 7.93 (dd, 1H), 8.03 (dd, 1H), 8.04 (dd, 1H), 8.05 (d, 1H) 8.50 (dd, 1H), 8.58 (d, 1H), 10.17 (d, 2H), 10.24 (d,1H). IR: $\tilde{\nu}$ = 1118 s (νSO) cm^{-1}.

***mer*-[RhCl$_3$(DMSO)(dpq)] 3a.** Synthesis as for **1a** with dipyrido[3,2-*f*:2′,3′-*h*]quinoxaline (104.7 mg, 0.45 mmol). Yield: 76%. Anal. ($C_{16}H_{14}Cl_3N_4ORhS$) C, H, N. LSIMS: m/z (%) 483(28) [M − Cl]$^+$, 405(9) [M − Cl − DMSO]$^+$, 370(100) [M − 2Cl − DMSO]$^+$, 335(83) [M − 3Cl − DMSO]$^+$. ^{1}H NMR ($CDCl_3$) δ: 3.84 (s, 6H, CH_3), 8.13 (dd, 1H), 8.23 (dd, 1H), 9.19 (s, 2H), 9.70 (d, 1H) 9.78 (d, 1H), 10.33 (d, 1H), 10.39 (d, 1H). IR: $\tilde{\nu}$ = 1118 s (νSO) cm^{-1}.

***mer*-[RhCl$_3$(DMSO)(dppz)]$\cdot$1.5H$_2$O 4a.** Synthesis as for **1a** with dipyrido[3,2-*a*:2′,3′-*c*]phenazine (127.3 mg, 0.45 mmol). Yield: 71%. Anal. ($C_{20}H_{19}Cl_3N_4O_{2.5}RhS$) C, H, N. LSIMS: m/z (%) 533(19) [M − Cl]$^+$, 458(9) [M − Cl − DMSO]$^+$, 420(65) [M − 2Cl − DMSO]$^+$, 385(100). ^{1}H NMR ($CDCl_3$) δ: 3.75 (s, 6H, CH_3) 8.00 (dd, 1H), 8.02 (dd, 1H), 8.11 (s, 1H), 8.13 (s, 1H) 8.38 (d, 1H), 8.40 (d, 1H), 9.76 (d, 1H), 9.82 (d,1H), 10.22 (d, 1H), 10.28 (d, 1H) ppm. IR: $\tilde{\nu}$ = 1130 s (νSO) cm^{-1}.

***mer*-[RhCl$_3$(DMSO)(dppn)] 5a.** Synthesis as for **1a** with benzo[i]dipyrido[3,2-*a*:2′,3′-*c*]phenazine (149.6 mg, 0.45 mmol). Yield: 68%. Anal. ($C_{24}H_{18}Cl_3N_4ORhS$) C, H, N. LSIMS: m/z (%) 583(38) [M − Cl]$^+$, 548(11) [M − 2Cl]$^+$ 435(41) [M − 3Cl − DMSO]$^+$. ^{1}H NMR ($CDCl_3$) δ: 3.80 (s, 6H, CH_3) 7.68, 7.70 (2d, 2H), 8.07 (dd, 1H), 8.16 (dd, 1H), 8.25, 8.27 (2d, 2H) 9.06, 9.08 (2s, 2H), 9.80, 9.86 (2d, 2H), 10.25, 10.31 (2d, 2H). IR: $\tilde{\nu}$ = 1118 s (νSO) cm^{-1}.

[RhCl$_3$(DMSO){{(CH$_2$)$_2$S}$_2$}] 6. Synthesis as for **1a** with 1,4 dithiane (54.2 mg, 0.45 mmol). Yield: 40%. Anal. ($C_6H_{14}Cl_3ORhS_3$) C, H, S. LSIMS: m/z (%) 371(100) [M − Cl]$^+$, ^{1}H NMR ($CDCl_3$) δ: 3.43 (s, 3H, CH_3), 3.44, 3.50 (m,8H,CH_2), 3.55 (s,3H,CH_3). IR: $\tilde{\nu}$ = 1122 s (νSO) cm^{-1}.

Cytotoxicity Measurements. MCF-7 breast cancer and HT-29 human colon carcinoma cells were maintained in 10% (v/v) fetal calf serum containing cell culture medium (minimum essential eagle supplemented with 2.2 g $NaHCO_3$, 110 mg/L sodium pyruvate and 50 mg/L gentamicin sulfate adjusted to pH 7.4) at 37 °C/5% CO_2 and passaged twice a week according to standard procedures. The antiproliferative effects of **1a**−**6** were determined by an established procedure.[32] Cells were suspended in cell culture medium (MCF-7: 10000 cells/mL; HT-29: 2850 cells/mL), and 100 μL aliquots thereof were plated in 96 well plates and incubated at 37 °C/5% CO_2 for 72 h (MCF-7) or 48 h (HT-29). Stock solutions of the compounds in DMSO were freshly prepared and diluted with cell culture medium to the desired concentrations (final DMSO concentration: 0.1% v/v). The medium in the plates was replaced with the medium containing the compounds in graded concentrations (six replicates). After further incubation for 96 h (MCF-7) or 72 h (HT-29), the cell biomass was determined by crystal violet staining and the IC_{50} values were established as those concentrations causing 50% inhibition of cell proliferation. Results were calculated from 2−3 independent experiments.

Cellular Uptake Studies. For cellular uptake studies, HT-29 and MCF-7 cells were grown until at least 70% confluency in 175 cm^2 cell culture flasks. Stock solutions of complexes **1a**−**6** in DMSO were freshly prepared and diluted with cell culture medium to the desired concentrations (final DMSO concentrations: 0.1% v/v; final complex concentration: 0.2−5.0 μM). The cell culture medium of the cell culture flasks was replaced with 10 mL of the cell culture medium solutions containing **1a**−**6** and the flasks were incubated for 0−6 h at 37 °C/5% CO_2. Then the culture medium was removed, the cell layer washed with 10 mL PBS (phosphate buffered saline pH 7.4), treated with 2−3 mL trypsin solution (0.05% trypsin, 0.02% EDTA in PBS), and incubated for 2 min at 37 °C/5% CO_2 after removal of the trypsin solution. Cells were resuspended in 10 mL of PBS, and cell pellets were isolated by centrifugation (RT, 2000g, 5 min) The isolated cell pellets were resuspended in 1−5 mL of twice-distilled water, lysed by using a sonotrode, and approximately diluted using twice distilled water. The rhodium content of the samples was determined by atomic absorption spectroscopy (AAS, see below) and the protein content of separate aliquots by the Bradford method. To correct for matrix effects in AAS, measurements samples and standards were adjusted to the same protein concentration by dilution with twice-distilled water (matrix matched calibration). Prior to AAS analysis, 20 μL of Triton X-100 (1%) and 20 μL of nitric acid (13%) were added to each 200 μL sample of the cell suspensions. Cellular uptake was expressed as ng rhodium per mg cell protein for data obtained from 2−3 independent experiments. Conversion of the ng rhodium/mg protein value to the micromolar cellular concentration was performed as described previously.[21,22]

Atomic Absorption Spectroscopy. A Vario 6 graphite furnace atomic absorption spectrometer (Analytik Jena) was employed

for the Rh quantification using a wavelength of 343.5 nm with a bandpass of 0.5 nm. A deuterium lamp was used for background correction. Matrix containing standards were obtained by addition of a rhodium stock solution (1 mg/mL Rh in 5% HCl) to untreated cell suspensions. Probes were injected at a volume of 20 μL into standard graphite tubes. Drying, pyrolysis, and atomization in the graphite furnace was performed according to the conditions listed in Table S5 of the Supporting Information. During the temperature program the graphite tube was purged with a constant argon gas flow, which was only halted during the zeroing and atomization steps. Pyrolysis and atomization temperatures were optimized prior to the experiments and the recovery rates of the metallodrugs using the above-mentioned conditions were determined (data not shown). The mean recovery rate of the metallodrugs (74 ± 12%) was used for calculation of the final values. The mean integrated absorbances of duplicate injections were used throughout the study. The characteristical concentration for the described method was 0.85 ± 0.05 (μg Rh L^{-1})/1% A.

Cellular Metabolism. Changes in cellular metabolism and morphology were analyzed using a Bionas 2500 sensor chip system (Bionas, Rostock, Germany). The sensor chip allows to continuous measurement of three important parameters of cellular metabolism: oxygen consumption using oxygen sensitive electrodes, change in the pH of the medium using ion-sensitive field effect transistors and the impedance between two interdigitated electrode structures to register the impedance under and across the cell layer on the chip surface.[24–26] Before measurement, cells were seeded on the sensor chip in DMEM (PAA, E15-883) with penicillin/streptomycin and 10% (v/v) FCS (PAA) and incubated in a standard tissue culture incubator at 37 °C, 5% CO_2, and 95% humidity for 24 h until 90% confluency was reached. Sensor chips with cells were then transferred to the Bionas2500 analyzer in which medium is continously exchanged in 8 min cycles (4 min exchange of medium and 4 min without flow) during which the parameters were measured. The running medium used during analysis was DMEM without carbonate buffer and only weakly buffered with 1 mM Hepes and reduced FCS (0.1%). For drug activity testing, the three following steps were included: (a) 4 h equilibration with running medium with 4 min stop/flow incubation intervals, (b) 6 h drug incubation with substances freshly dissolved in medium at indicated concentrations also with 4 min stop/flow, and (c) a regeneration step in which cells are again fed with running medium without substances. At the end of each experiment, cells were killed by addition of 0.2% Triton X-100 to obtain a basic signal without living cells on the sensor surface as a negative control.

Acknowledgment. Financial support for this work in Berlin, Bochum, and Heidelberg by the Deutsche Forschungsgemeinschaft (DFG) within the research group FOR 630 "Biological function of Organometallic Compounds" is gratefully acknowledged. We are also grateful to Heike Mayer-Figge and Heike Scheffler for technical support.

Supporting Information Available: CD spectrum of a 1:10 **4a**/DNA mixture, figure with IC_{50} values for **1a**−**5a**, combustion material analysis data for **1a**−**6**, furnace program for AAS measurements. This material is available free of charge via the Internet at http://pubs.acs.org.

References

(1) Katsaros, N.; Anagnostopoulou, A. Rhodium and its compounds as potential agents in cancer treatment. *Crit. Rev. Oncol. Hematol.* **2002**, *42*, 297–308.

(2) Sorasaenee, K.; Fu, P. K. L.; Angelas-Boza, A. M.; Dunbar, K. R.; Turro, C. Inhibition of transcription in vitro by anticancer active dirhodium(II) complexes. *Inorg. Chem.* **2003**, *42*, 1267–1271.

(3) Angeles-Boza, A. M.; Chifotides, H. T.; Aguirre, J. D.; Chouai, A.; Fu, P. K. L.; Dunbar, K. R.; Turro, C. Dirhodium(II,II) complexes: molecular characteristics that affect in vitro activity. *J. Med. Chem.* **2006**, *49*, 6841–6847.

(4) Qu, P.; He, H.; Liu, X. Antitumor activity and mechanism of rhodium complexes. *Progr. Chem.* **2006**, *18*, 1646–1651.

(5) Mestroni, G.; Alessio, E.; Sessanti o Santi, A.; Geremia, S.; Bergamo, A.; Sava, G.; Boccarelli, A.; Schettino, A.; Coluccia, M. Rhodium(III) analogues of antitumor-ative ruthenium(II) compounds: the crystal structure of [ImH][*trans*-$RhCl_4(Im)_2$] (Im = imidazole). *Inorg. Chim. Acta* **1998**, *273*, 62–71.

(6) Colamarino, P.; Orioli, P. Crystal and molecular structure of trichloro(dimethyl sulphoxide)bis-pyridinerhodium(III). *J. Chem. Soc., Dalton Trans.* **1976**, 845–848.

(7) Pruchnik, F. P.; Jakimowicz, P.; Ciunik, Z.; Zakrzewska-Czerwińska, J.; Opolski, A.; Wietrzyk, J.; Wojdat, E. Rhodium(III) complexes with polypyridyls and pyrazole and their antitumor activity. *Inorg. Chim. Acta* **2002**, *334*, 59–66.

(8) Medvetz, D. A.; Stakleff, K. D.; Schreiber, T.; Custer, P. D.; Hindi, K.; Panzner, M. D.; Blanco, D. D.; Taschner, M. J.; Tessier, C. A.; Youngs, W. J. Ovarian cancer activity of cyclic amines and thiaether metal complexes. *J. Med. Chem.* **2007**, *50*, 1703–1706.

(9) Schäfer, S.; Ott, I.; Gust, R.; Sheldrick, W. S. Influence of the polypyridyl(pp) ligand size on the DNA binding properties, cytotoxicity and cellular uptake of organoruthenium(II) complexes of the type $[(\eta^6\text{-}C_6Me_6)Ru(L)(pp)]^{n+}$ [L = Cl, n = 1; L = $(NH_2)_2CS$, n = 2]. *Eur. J. Inorg. Chem.* **2007**, 3034–3046.

(10) Scharwitz, M.; Ott, I.; Geldmacher, Y.; Gust, R.; Sheldrick, W. S., Cytotoxic half-sandwich rhodium(III) complexes: polypyridyl ligand influence on their DNA binding properties and cellular uptake. *J. Organomet. Chem.* **2008**, DOI 10.1016/j.jorganchem.2008.04.002.

(11) Schäfer, S.; Sheldrick, W. S. Coligand tuning of the DNA binding properties of half-sandwich organometallic intercalators: influence of polypyridyl(pp) and monodentate ligands (L = Cl, $(NH_2)_2CS$, $(NMe_2)_2CS$) on the intercalation of (η^5-pentamethylcyclopentadienyl) iridium(III)-dipyridoquinoxaline and -dipyridophenazine complexes. *J. Organomet. Chem.* **2007**, *692*, 1300–1309.

(12) Messori, L.; Marcon, G.; Orioli, P.; Fontani, M.; Zanello, P.; Bergamo, A.; Sava, G.; Mura, P. Molecular structure, solution chemistry and biological properties of the novel [ImH][trans-$IrCl_4(DMSO)$], (I) and of the orange form of $[(DMSO)_2H][trans\text{-}IrCl_4(DMSO)_2]$, (II), complexes. *J. Inorg. Biochem.* **2003**, *95*, 37–46.

(13) Sokol, V. I.; Porai-Koshits, M. A. Coordination of dimethyl sulfoxide in rhodium(III) complexes. Crystal and molecular structure of tris-(dimethylsulfoxide)trichlororhodium. *Sov. J. Coord. Chem.* **1975**, *1*, 577–583.

(14) James, B. R.; Morris, R. H. Sulfur-bonded sulfoxide complexes of rhodium(III) and rhodium(I). *Can. J. Chem.* **1980**, *58*, 399–408.

(15) Alessio, E.; Faleschini, P.; Sessanta o Santi, A.; Mestroni, G.; Calligaris, M. A new linkage isomer of $RhCl_3(DMSO)_3$: photochemical synthesis, crystal structure, and activity of *mer*,*trans*-$[RhCl_3(DMSO)_2(DMSO)]$. *Inorg. Chem.* **1993**, *32*, 5756–5761.

(16) Herebian, D.; Sheldrick, W. S. Synthesis and DNA binding properties of bioorganometallic (η^5-pentamethylcyclopentadienyl)iridium(III) complexes of the type $[(\eta^5\text{-}C_5Me_5)Ir(Aa)(dppz)]^{n+}$ (dppz = dipyrido[3,2-*a*:2′,3′-*c*]phenazine, n = 1−3), with S-coordinated amino acids (Aa) or peptides. *J. Chem. Soc., Dalton Trans.* **2002**, 966–974.

(17) Gencaslan, S.; Sheldrick, W. S. Bifunctional bioorganometallic iridium(III)−platinum(II) complexes incorporating both intercalative and covalent DNA binding capabilities. *Eur. J. Inorg. Chem.* **2005**, 3840–3849.

(18) Frodl, A.; Herebian, D.; Sheldrick, W. S. Coligand tuning of the DNA binding properties of bioorganometallic (η^6-arene)ruthenium(II) complexes of the type $[(\eta^6\text{-arene})Ru(amino\ acid)(dppz)]^{n+}$ (dppz = diyrido[3,2-*a*:2′,3′-*c*]phenazine), n = 1−3. *J. Chem. Soc., Dalton Trans.* **2002**, 3664–3674.

(19) Brabec, V.; Kleinwächter, V.; Butour, J.-L.; Johnson, N. P. Biophysical studies of the modification of DNA by antitumor platinum coordination complexes. *Biophys. Chem.* **1990**, *35*, 129–141.

(20) Eriksson, M.; Nordén, B. Linear and circular dichroism of drug-nucleic acid complexes. *Methods Enzymol.* **2001**, *340*, 68–98.

(21) Ott, I.; Scheffler, H.; Gust, R. Development of a method for the quantification of the molar gold concentration in tumour cells exposed to gold-containing drugs. *ChemMedChem* **2007**, *2*, 702–707.

(22) Gust, R.; Schnurr, B.; Krauser, R.; Bernhardt, G.; Koch, M.; Schmid, B.; Hummel, E.; Schönenberger, H. Stability and cellular studies of [*rac*-1,2-bis-(4-fluorophenyl)-ethylenediamine][cyclobutane-1,1-dicarboxylato] platinum(II), a novel, highly active carboplatin derivative. *J. Cancer Res. Clin. Oncol.* **1998**, *124*, 585–597.

(23) Ghezzi, A. R.; Aceto, M.; Cassino, C.; Gabano, E.; Osella, D. Uptake of antitumor platinum (II) complexes by cancer cells, assayed by inductively coupled plasma mass spectrometry (ICP-MS). *J. Inorg. Biochem.* **2004**, *98*, 73–78.

(24) Wolf, B.; Brischwein, M.; Baumann, W.; Ehret, R.; Kraus, M. Monitoring of cellular signalling and metabolism with modular server-technique: The PhysioControl-Microsystem (PCM). *Biosens. Bioelectron.* **1998**, *13*, 501–509.

(25) Lehmann, M.; Baumann, W.; Brischwein, M.; Ehret, R.; Kraus, M.; Schwinde, A.; Bitzehofer, M.; Freud, I.; Wolf, B. Non-invasive measurement of cell membrane associated proton gradients by ion-sensitive field effect transistor arrays for microphysiological and bioelectronical applications. *Biosens. Bioelectron.* **2000**, *15*, 117–124.

(26) Ehret, R.; Baumann,W.; Brischwein, M.; Schwinde, A.; Wolf, B. On-line control of cellular adhesion with impedance measurements using interdigitated electrode structures. *Med. Biol. Eng. Comput.* **1998**, *36*, 365–370.

(27) Merino, E. J.; Barton, J. K. DNA oxidation by charge transport in mitochondria. *Biochemistry* **2008**, *47*, 1511–1517.

(28) Collins, J. G.; Sleemann, A. D.; Aldrich-Wright, J. R.; Greguric, I.; Hambley, T. W. A ^{1}H NMR study of the DNA binding of ruthenium(II) polypyridyl complexes. *Inorg. Chem.* **1998**, *37*, 3133–3141.

(29) Delgadillo, A.; Romo, P.; Leiva, A. M.; Loeb, B. Synthesis and characterization of ruthenium complexes with substituted pyrazino[2,3-*f*][1,10]-phenanthroline (= Rppl; R = Me, COOH, COOMe). *Helv. Chim. Acta* **2003**, *86*, 2110–2120.

(30) Yam, Y. W.-W.; Lo, K. K.-W.; Cheung, K.-K.; Kong, R. Y.-C. Synthesis, photophysical properties and DNA binding studies novel luminescent rhenium(I) complexes: X-ray crystal structure of [Re(dppn)$(CO)_3$(py)](OTf). *J. Chem. Soc., Chem. Commun.* **1995**, 1191–1193.

(31) Sheldrick, G. M. *SHELXS97 and SHELXL97*; Göttingen, Germany, 1997.

(32) Ott, I.; Schmidt, K.; Kircher, B.; Schuhmacher, P.; Wiglenda, T.; Gust, R. Antitumor-active cobalt−alkyne complexes derived from acetylsalicylic acid: studies on the mode of drug action. *J. Med. Chem.* **2005**, *48*, 622–629.

JM800173S